

SPECTRAL RETRIEVAL OF LATENT HEATING PROFILES FROM TRMM PR DATA: ALGORITHM IMPROVEMENT AND HEATING ESTIMATES OVER TROPICAL OCEAN REGIONS

Shoichi Shige^{1,*}, Yukari N. Takayabu², Wei-Kuo Tao³ and Chung-Lin Shie^{3,4}

¹Department of Space Engineering, Osaka Prefecture University, Osaka, Japan

²Center for Climate System Research, University of Tokyo, Tokyo, Japan

³Laboratory for Atmospheres, NASA/Goddard Space Flight Center, Greenbelt, Maryland, U.S.A.

⁴Goddard Earth Sciences and Technology Center, University of Maryland, Baltimore County, Baltimore, Maryland, U.S.A.

1. INTRODUCTION

The precipitation radar (PR) of the TRMM provides height information based upon the time delay of the precipitation-backscattered return power, and has enabled us to directly obtain vertical profiles of precipitation over the global Tropics (Kozu et al., 2001; Okamoto, 2003). The classification between convective and stratiform regions of mesoscale convective systems (MCS) became more straightforward utilizing observed precipitation profiles (Awaka et al., 1998). The accuracy of this classification is very important for estimating latent heating, because the differences of diabatic heating profiles that exist between convective and stratiform regions of MCSs (Houze, 1982; Johnson and Young, 1983). For convective regions of MCSs the heating profile has warming at all levels with a maximum at midlevels, whereas in stratiform regions there is a warming peak in the upper troposphere and a cooling peak at low-levels. The resulting MCS heating profile is positive at all levels, but with a maximum value in the upper troposphere.

Takayabu (2002) obtained a spectral expression of precipitation profiles to examine convective and stratiform rain characteristics statistically over the equatorial area (10°N-10°S) observed by the TRMM PR. In her study, all nadir data of PR2A25 version 5 (Iguchi et al. 2000) for the period of 1998-1999 were utilized and convective and stratiform precipitation were separated based on the TRMM PR version 5 2A23 convective-stratiform separation algorithm. Precipitation profiles with 0.3 mm hr⁻¹ precipitation-top threshold were accumulated and stratified with precipitation-top heights (PTHs). Properties of convective rain profiles show near monotonic change with cumulative frequency. Stratiform rain profiles

consist of two groups. One group consists of shallow stratiform rain profiles which are very weak and increase downward. The other group consists of anvil rain profiles, characterized by maximum intensity around the melting level, much less intensity above, and a downward decrease below as indicated in traditional radar observations.

Based on the results of spectral precipitation statistics of Takayabu (2002), the Spectral Latent Heating (SLH) algorithm has been developed for the TRMM PR (Shige et al. 2004, hereafter S2004). Heating profile lookup tables for the three rain types— convective, shallow stratiform, and anvil rain (deep stratiform with a melting level) were produced with numerical simulations of tropical cloud systems in Tropical Ocean Global Atmosphere (TOGA) Coupled Ocean–Atmosphere Response Experiment (COARE) utilizing a cloud-resolving model (CRM). For convective and shallow stratiform regions, the lookup table refers to the precipitation top height (PTH). For anvil region, on the other hand, the lookup table refers to the precipitation rate at the melting level instead of PTH.

It is necessary to examine the universality of the lookup table for global application of the SLH algorithm to TRMM PR data. If relationship between precipitation profiles and associated latent heating profiles change between regions, the lookup table would produce large error. In this study, we compare the lookup table from TOGA-COARE, GARP Atlantic Tropical Experiment (GATE), South China Sea Monsoon Experiment (SCSMEX) and Kwajelin Experiment (KWAJEX) simulations to examine its universality.

2. APPROACH

Due to the scarcity of reliable validation data and difficulties associated with the collocation of validation data and satellite measurements, a consistency check of the SLH algorithm is performed, us-

*Corresponding author address: Dr. Shoichi Shige, Department of Space Engineering, Osaka Prefecture University, 1-1 Gakuen-cho, Sakai, Osaka, 599-8531 Japan; e-mail: shige@aero.osakafu-u.ac.jp

ing CRM-simulated precipitation profiles as a proxy for the PR data. The algorithm-reconstructed heating profiles from CRM-simulated precipitation profiles are compared to CRM-simulated “true” heating profiles, which are computed directly from the model thermodynamic equation. Here the 2-D version of the Goddard Cumulus Ensemble (GCE) model (Tao and Simpson, 1993) is used. Numerical simulations were conducted with the large-scale forcing data from TOGA-COARE, GATE, SCSMEX and KWAJEX. In this paper, the SLH algorithm is also applied to PR data and the results will be compared to heating profiles derived diagnostically from sounding data of SCSMEX (Johnson and Ciesielski, 2002). We will show the results with $Q_1 - Q_R$ (Q_{1R}), which is the important dynamically important quantity. Here Q_1 is the apparent heat source defined in diagnostic studies (Yanai et al., 1973; Yanai and Johnson, 1993), and Q_R is the cooling/heating rate associated with radiative processes.

3. ALGORITHM IMPROVEMENT

3.1. Consistency check of the original algorithm

In addition to an episode from TOGA-COARE (19–26 December 1992) as shown in S2004, three episodes from GATE (September 1–8 1974), SCSMEX (June 2–9 1998) and KWAJEX (September 6–13 1999) are used for a consistency check of the SLH algorithm (Fig. 1).

The SLH1 algorithm with COARE lookup table produces excellent agreement between SLH-algorithm reconstructed and GCE simulated heating profiles for COARE (Fig. 1a), as shown in S2004. It may be noticed that the SLH1-reconstructed convective heating above the freezing level is slightly stronger than GCE-simulated one. This is because the simulated data used for the construction of lookup tables includes that from the two subperiods with 9-day durations (9–17 February 1993, and 18–26 February 1993) of which convection has stronger heating above the freezing level than that of the 19–26 December 1992 period. This is consistent with the result of DeMotte and Rutledge (1998a,b) who reported that convection of cruise 3 (29 Jan 1993–25 February 1993) has greater liquid and ice water masses above the freezing level than that of cruise 2 (21 December 1992–19 January 1993) using radar data.

On the other hand, the COARE lookup table produces less agreement between SLH1-reconstructed and GCE-simulated heating profiles for GATE convective and stratiform regions (Fig. 1b). The SLH1-reconstructed heating at $z = 4–6$ km is stronger than the GCE model-simulated one for convective heat-

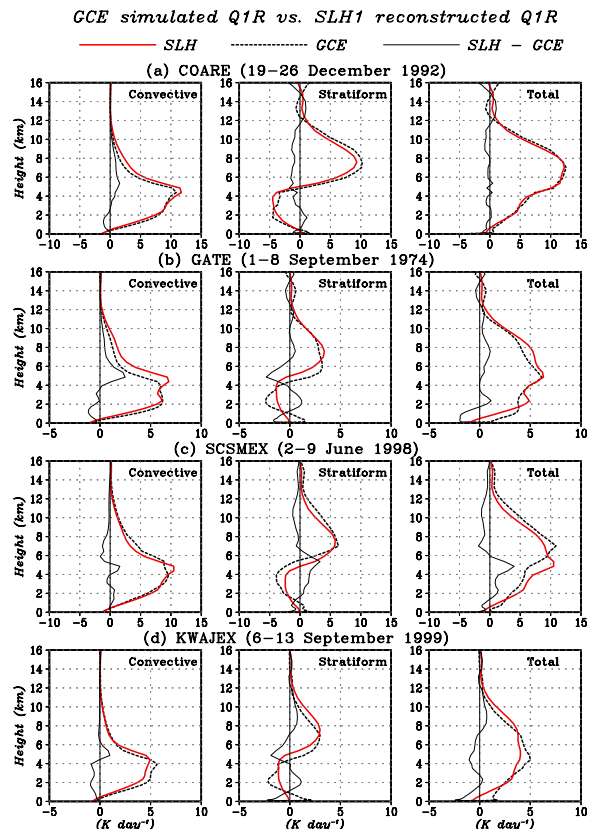


Figure 1: Eight-day averaged profiles of Q_{1R} reconstructed by the original SLH algorithm (SLH1) with the COARE lookup table (thick solid line) and simulated by the GCE model (dotted line) for (a) COARE (19–26 December 1992) case, (b) GATE (September 1–8 1974) case, (c) SCSMEX (June 2–9 1998) and (d) KWAJEX (September 6–13 1999), respectively. Left panels for convective regions, center panels for stratiform regions, and right panels for total regions. Thin solid line indicates differences between the SLH1-reconstructed and the GCE-simulated.

ing profiles, while the SLH1 algorithm reconstructs cooling at $z = 4–6$ km where the GCE model simulates heating for stratiform heating profiles. The reconstructed total heating is in good agreement with simulated one. Compensation of error at $z = 4–6$ km for each component (convective and stratiform) is the reason for this good agreement. A separation of convective and stratiform heating profile estimates is very important, thus an algorithm improvement is needed.

The COARE lookup table produces better agreement between reconstructed and simulated heating profiles for SCSMEX convective region than for GATE convective region (Fig. 1c). It is noticed that the SLH1-reconstructed convective heating decrease more rapidly with height above the freezing level than the GCE simulated one does. However,

the reconstructed total heating is in poorer agreement with simulated one for SCSMEX than for GATE. The level of heating maximum of reconstructed total heating profile is about 5 km, while that of simulated total heating profile is about 7 km. This is because the SLH1 algorithm reconstructs cooling at $z = 4\text{--}6$ km where the GCE model simulates heating for stratiform heating profiles and error for each component does not compensate.

The SLH1-reconstructed heating at $z = 4\text{--}6$ km is stronger than the GCE model-simulated one for KWAJEX total heating profile (Fig. 1d). This difference is mainly due to the disagreement between reconstructed and GCE simulated heating profiles for stratiform region where the SLH1 algorithm reconstructs cooling at $z = 4\text{--}5$ km where the GCE model simulates heating. Thus the algorithm improvement is needed for the stratiform region.

3.2. Comparisons of lookup tables

Figure 2a–d show lookup tables for convective rain produced from COARE, GATE, SCSMEX and KWAJEX simulations. The GCE-simulated precipitation profiles with a 0.3 mm h^{-1} precipitation-top threshold and corresponding heating profiles are accumulated and averaged for each PTH with model grid intervals. Two episodes from SCSMEX (18–26 May 1998 and 2–11 June 1998), two episodes from GATE (September 1–8 1974 and Sep 9–18 1974), and three episode KWAJEX (7–11 August 1999, 17–20 August, 29 August–5 September and 6–12 September) are used in order to increase the number of sample profiles.

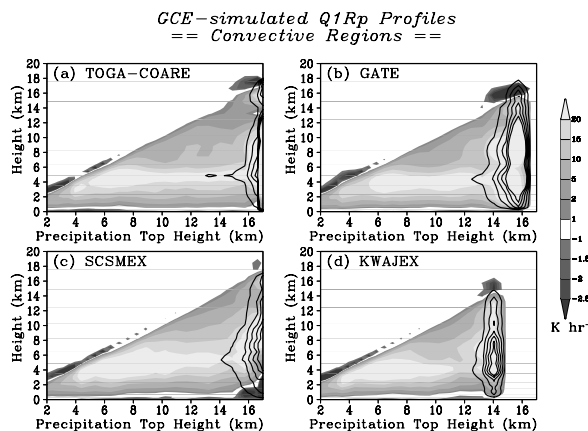


Figure 2: Ensemble-mean, GCE-simulated Q_{1R} profiles, plotted as functions of precipitation top height (PTH) from convective regions for (a) COARE, (b) GATE, (c) SCSMEX, and (d) KWAJEX cases. Contours indicate values of confidence interval for the mean at the 95 % level with Student's-t test. Contour interval is 2.0 K h^{-1} .

The similarity of lookup table from case to case can be seen. Properties of convective heating profiles show near-monotonic changes with PTH. The shallow convective heating profiles ($\text{PTH} < 6 \text{ km}$) are characterized by a cooling aloft due to an excess of evaporation over condensation, such as tradewinds cumulus (Nitta and Esbensen, 1974). Another interesting feature is that the convective heating profiles with highest PTH are characterized by a cooling aloft. This feature is consistent with strong cooling above the mesoscale convective system observed by Johnson and Kriete (1982) and Lin and Johnson (1996b). On the other hand, there exists internal variations in vertical structure (e.g. the level of Q_{1R} heating maximum) for a given PTH. These accounts for the differences between the SLH1-reconstructed convective heating profiles and GCE-simulated ones seen in Fig. 1. Note that confidence level of heating profiles with PTH higher than 15 km (14 km) from GATE (KWAJEX) simulations for the mean is low because of the small number of profiles.

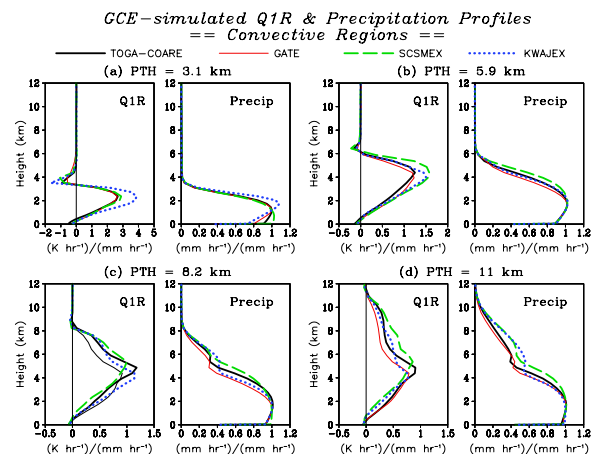


Figure 3: Ensemble-mean, GCE-simulated Q_{1R} and precipitation profiles, with precipitation top height (PTH) of (a) 3.1 km, (b) 5.9 km, (c) 8.2 km, and (d) 11 km from convective regions for COARE, GATE, SCSMEX, and KWAJEX cases. Note that Q_{1R} profiles and precipitation profiles are normalized by near-surface rainrate.

Figure 3 shows GCE-simulated Q_{1R} and precipitation profiles, with precipitation top height (PTH) of 3.1 km, 5.9 km, 8.2 km, and 11 km from convective regions for COARE, GATE, SCSMEX, and KWAJEX cases. Note that Q_{1R} profiles and precipitation profiles are normalized by near-surface rainrate. Heating top height is determined by PTH and the heating depth for a given PTH does not vary from location to location. The vertical structure (e.g., heating maximum level) of the shallow convective heating profiles ($\text{PTH} = 3.1 \text{ km}$) does not vary from location to location. However, the differences in convective heat-

ing profile shape among cases increased with PTH. COARE convection provides stronger latent heating above the melting level than GATE and KWAJEX convection does, but weaker one than SCSMEX convection does. These differences are largest in the deeper convective heating profiles (PTH > 8.2 km). These differences in the vertical distribution of deeper convective heating account for the discrepancies for convective region in the consistency check (Fig. 1).

Similarly, the differences in corresponding precipitation profile shape among cases also increased with PTH. COARE convection provides stronger precipitation intensity above the freezing level than GATE and KWAJEX convection does, but weaker one than SCSMEX convection does. Thus, the systematic variability of heating and precipitation profiles due to the relative importance of liquid water and ice processes is found above the freezing level. Convective cells with enhanced liquid water processes have latent heating and precipitation concentrated below the freezing level, whereas convective cells with significant ice processes provide stronger latent heating and more precipitation above the freezing level. Thus the precipitation profiles may be indicative of convective heating profile shape.

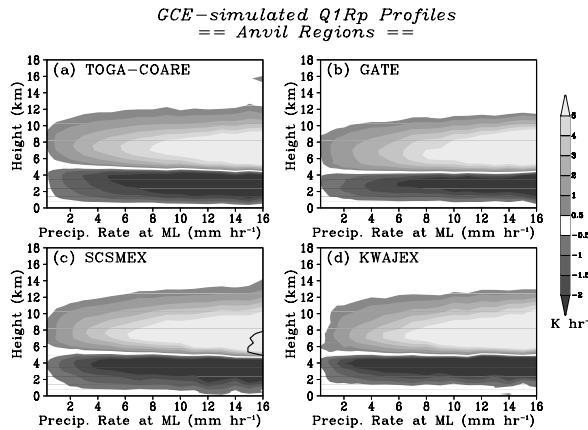


Figure 4: Lookup tables for the stratiform region produced from (a) COARE, (b) GATE, (c) SCSMEX and (d) KWAJEX simulations.

This is consistent with the results of Petersen and Rutledge (2001) who found the largest systematic variability in precipitation vertical structure between tropical locations above the freezing level using the TRMM PR and Lightning Imaging Sensor (LIS) observations. Furthermore, they pointed out that slight increases in convective intensity are present over South China Sea (i.e. SCSMEX) relative to isolated ocean regimes (i.e. COARE, GATE, KWAJEX) while convection over western Pacific warm pool (i.e. COARE) is slightly more intense than that sampled

over other ocean (i.e. GATE, KWAJEX). Thus, the aforementioned differences among COARE, GATE, SCSMEX, and KWAJEX may be consistent with their results.

Fig. 4a–d show lookup tables for anvil (deep stratiform with a melting level) rain produced from COARE, GATE, SCSMEX and KWAJEX simulations. The similarity of anvil heating profiles among lookup tables from case to case can be seen, although there are differences of the level separating upper-level heating and lower-level cooling due to those of the melting level. These results agree well with observations of stratiform heating profiles summarized in Houze (1989) who concluded that stratiform heating profiles are not substantially different from one location to the next.

3.3. Revised procedure for heating retrieval

Comparisons of convective lookup tables suggested that the variability of heating profiles above the freezing level should be taken into account for convective heating retrieval. Hence, upper-level heating amplitude due to ice processes and lower-level heating amplitude due to liquid water processes are determined separately in the revised procedure of convective heating retrieval (Fig. 5). Based on some sensitivity tests, the level separating upper-level heating and lower-level heating is determined that 1 km above the melting level.

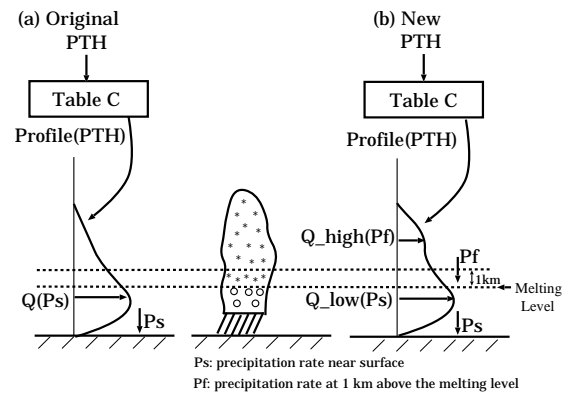


Figure 5: Diagram showing the procedure for deriving convective heating profiles using the spectral latent heating (SLH) algorithm. See the text for details.

The upper-level heating due to ice processes is determined by

$$Q(z)_{high} = \frac{\tilde{Q}_{high}(z)}{\tilde{P}_f} \cdot P_f. \quad (1)$$

where P_f is the precipitation rate at the level separating upper-level heating and lower-level heating and tildes denote the variables in the lookup table. On

the other hand, the lower-level heating due to liquid water processes is determined by

$$Q(z)_{low} = \frac{\tilde{Q}_{low}(z)}{\tilde{P}_s} \cdot P_s, \quad (2)$$

where P_s is the precipitation rate at the observable lowest level. This revised procedure shown in Fig. 5b is only applied to convective rain with PTHs which are 3 km higher than the level separating upper-level heating and lower-level heating. The original procedure shown in Fig. 5a is applied to the remaining convective rain.

For stratiform regions, we shift up or down the heating profile by matching the melting level of COARE lookup table with observed one.

3.4. Consistency check of the revised algorithm

Again, the four periods from TOGA-COARE (19–26 December 1992), GATE (Sep 1–8 1974), SCSMEX (Jun 2–9 1998) and KWAJEX (Sep 6–13 1999) are used for the consistency check of the revised SLH algorithm (hereafter SLH2) as shown in Fig. 6.

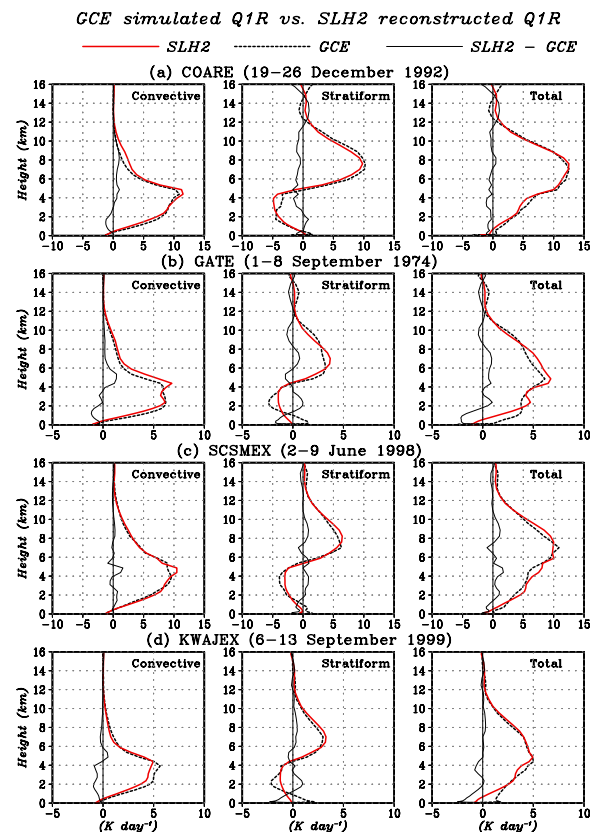


Figure 6: Same as Fig. 1, but reconstructed by the revised SLH algorithm (SLH2) with the COARE lookup table and simulated by the GCE model. Thin solid line indicates differences between the SLH2-reconstructed and the GCE-simulated.

For the COARE period, the SLH2-reconstructed heating profiles for the convective, stratiform, and total regions are almost identical to those reconstructed by the SLH1 algorithm. Actually, the SLH2-reconstructed heating profile for the stratiform region is exactly the same as the SLH1-reconstructed one because adjustment of the melting level is not needed. The SLH2-algorithm produces slightly weaker convective heating at $z = 5-6.5$ km than the SLH1-algorithm does and is in better agreement with the GCE model.

Although the total heating profile reconstructed by the SLH2 algorithm is almost identical to that reconstructed by the SLH1 algorithm for GATE, the error in each component is reduced. For the convective region, the SLH2-algorithm produces weaker heating above $z = 5$ km than the SLH1 algorithm does and is in much better agreement with the GCE model. For the stratiform region, the discrepancy in the level separating upper-level heating from lower-level cooling as reconstructed by the SLH2 algorithm and simulated by the GCE model is reduced.

For SCSMEX, the SLH2-algorithm produces stronger convective heating above $z = 5$ km than the SLH1 algorithm does, different from the COARE and GATE periods, and in very good agreement with the GCE model. For the stratiform region, the discrepancy in the level separating upper-level heating from lower-level cooling as reconstructed by the SLH2 algorithm and simulated by the GCE model is reduced such that very good agreement is obtained between the two heating profiles. As a result of the improvements in the convective and stratiform estimates, the total heating profile reconstructed by the SLH2 algorithm is in very good agreement with that simulated by the GCE model. The level of maximum heating reconstructed by SLH2 agrees with the GCE-simulated one.

For KWAJEX, the better agreement between the total heating profile reconstructed by the SLH2 algorithm and that simulated by the GCE model is explained by the fact that the discrepancy between the level separating upper-level heating from lower-level cooling as reconstructed by the SLH2 algorithm and simulated by the GCE model is reduced in the stratiform region. Still, the SLH2-algorithm produces slightly weaker convective heating at $z = 5-6$ km than the SLH1-algorithm does in better agreement with the GCE model.

4. PR APPLICATIONS

4.1. Validation with SCSMEX-NESA radiosonde networks

The accuracy of the SLH-retrieved heating can be evaluated by comparing with a rawinsonde-based

analysis of diabatic heating for the SCSMEX NESA derived by Johnson and Ciesielski (2002). Figure 7 shows a comparison between SLH-retrieved Q_{1Rp} from version 6 of the TRMM PR data sets and sounding-based Q_1 during the campaign's most convectively active period (May 15 – Jun 20 1998). Mapes et al. (2003) suggested that averages of about 30 days reduce sampling errors in the rainfall rate estimate (proportional to integrated Q_1 or Q_2) to 10 % for the SCSMEX NESA. There is good agreement in several key features of the vertical profiles, particularly the level of maximum heating. The SLH-retrieved Q_{1Rp} heating magnitudes are somewhat greater than the sounding-derived magnitudes. This difference is mainly caused by the fact the SLH-retrieved Q_{1Rp} does not include Q_R which is included in the sounding-derived Q_1 . Tao et al. (2003, 2004) reported that net radiation (cooling) accounts for about 20 % or more of the net condensation for the SCSMEX cloud systems simulated by the GCE model. The vertical profile of Q_R simulated by the GCE model for the SCSMEX periods (18–26 May 1998 and 2–11 June 1998) is shown on the left side of the figure. This Q_R component is added to the SLH-retrieved Q_{1Rp} estimates. The level of maximum heating of $Q_{1Rp} + Q_R$ and its magnitude are in very good agreement with the sounding-derived Q_1 .

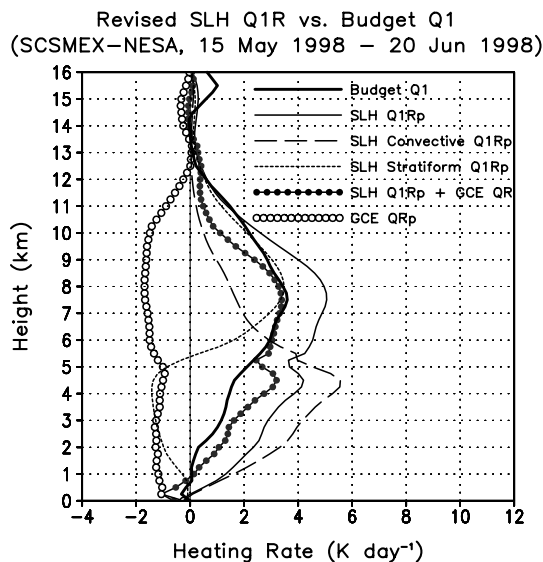


Figure 7: Heating from diagnostic calculations (Johnson and Ciesielski, 2002) and the SLH2 algorithm using version 6 of the TRMM PR data sets for SCSMEX (15 May - 20 June 1998).

Figure 7 shows that in the lower troposphere, the $Q_{1Rp} + Q_R$ heating magnitudes are somewhat greater than the sounding-derived magnitudes, because the SLH-estimated convective $Q_{1Rp} + Q_R$ heating magnitudes are larger than the SLH-

estimated stratiform $Q_{1Rp} + Q_R$ cooling magnitudes. Heating estimates from PR data are subject to sampling errors due to the PR's narrow swath width, leading to a discrepancy with the sounding estimates. Figure 8 presents a histogram of surface rain rates estimated by the TMI (i.e., 2A12 version 6) over the PR swath (~ 215 km) and over the full TMI swath (~ 760 km). The occurrence of moderate-to-heavy rain rates (≥ 5 mm h^{-1}) is more for the PR swath than for the TMI swath. These moderate-to-heavy rain pixels are classified mostly as convective rain. The heating estimates are sensitive to the estimated fraction of stratiform rainfall from the PR data. Thus, sampling errors may account for the overestimation of $Q_{1Rp} + Q_R$ heating in the lower troposphere.

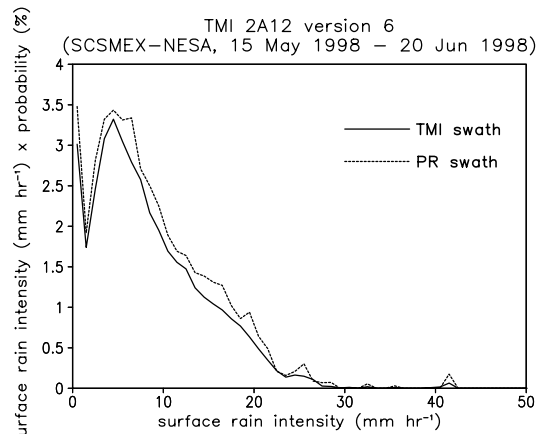


Figure 8: Contribution to total rainrate as a function of the surface rain intensity estimated by TMI 2A12 version 6 over the PR swath (~ 215 km) and over the full TMI swath (~ 760 km).

It is also evident from Fig. 7 that the $Q_{1Rp} + Q_R$ heating magnitudes are smaller than the sounding-derived magnitudes above 9 km. One possible source of error is the uncertainty in the PR ice-phase precipitation retrieval. The PR is a single frequency (13.8 GHz) radar and thus is insensitive to ice particles unless they are large enough to be detectable by 2.2-cm wavelength microwaves. In the future, the National Aeronautics and Space Administration (NASA) and Japan Aerospace Exploration Agency (JAXA), in collaboration with a number of other space agencies, plan to launch the Global Precipitation Measurement (GPM) mission. This mission would consist of a core satellite carrying a spaceborne dual-frequency precipitation radar with an additional channel at 35 GHz, as well as a passive microwave radiometer. The dual-frequency precipitation radar could improve upon ice-phase precipitation retrieval, resulting in an improvement in the SLH heating estimates.

4.2. Comparison with the CSH algorithm

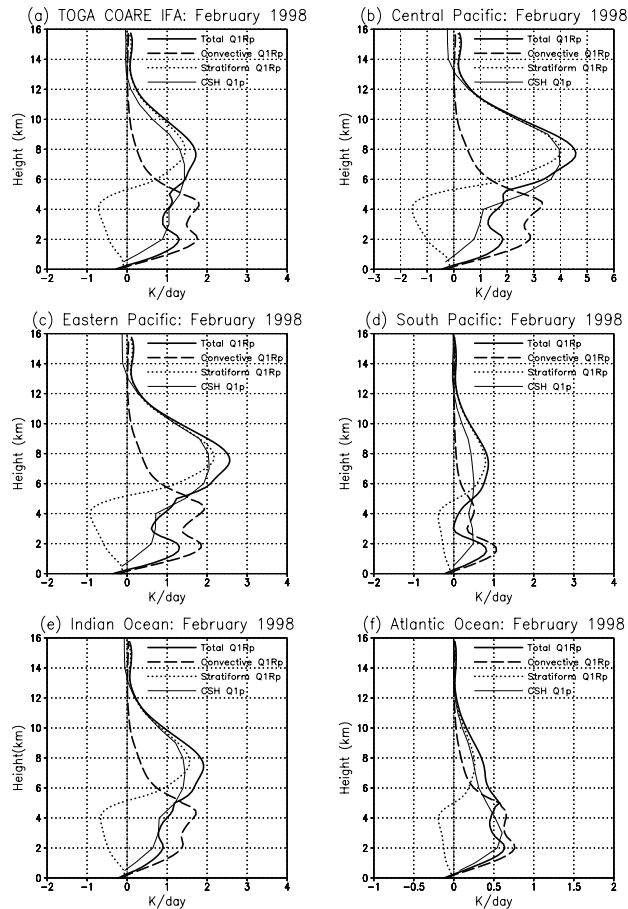


Figure 9: Monthly (February 1998) mean total, convective and stratiform heating profiles derived from the SLH2 algorithm for various locations. Total heating profiles derived from the CSH algorithm are also shown. The geographic areas are the (a) TOGA COARE IFA, (b) central Pacific, (c) east Pacific, (d) south Pacific, (e) Indian Ocean, and (f) Atlantic Ocean. Note that the abscissa scales for Figs. 9a–f are not always the same.

Tao et al. (2001) represented the first attempt at using version 5 TRMM rainfall products to estimate the latent heating structure over the global Tropics for February 1998, corresponding to the warm phase (El Niño) of the 1997/1998 El Niño–Southern Oscillation (ENSO). Three different latent heating algorithms, the hydrometeor heating (HH; Yang and Smith 1999a,b), the convective-stratiform heating (CSH; Tao et al. 1993, 2000), and the Goddard profiling (GPROF) heating (Olson et al. 1999) algorithms were used, and their results were intercompared. Only one of the three algorithms, the CSH algorithm can use PR products as input (CSH can also use the TMI products). The SLH algorithm performance is compared with the CSH algorithm using version

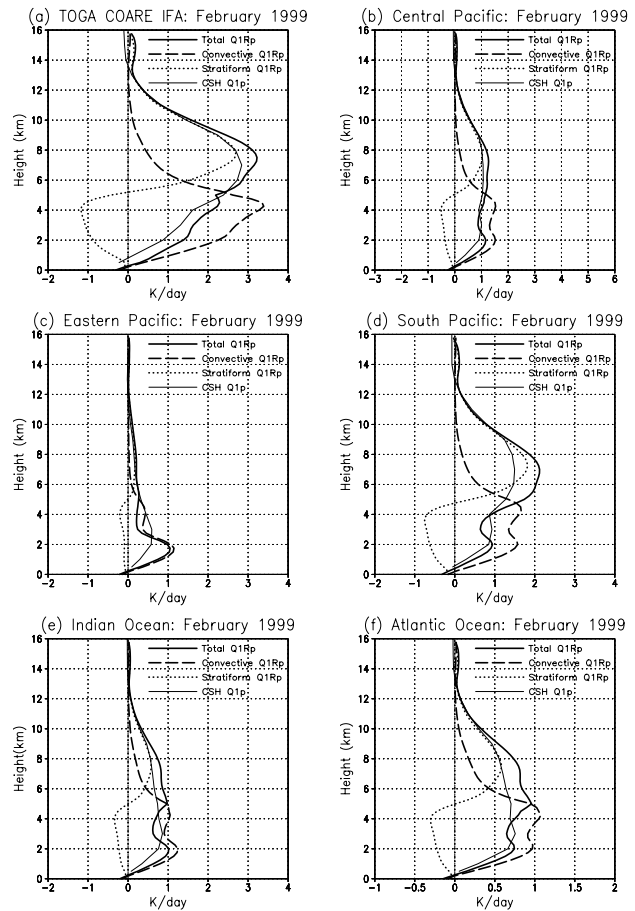


Figure 10: Same as Fig. 9 except for February 1999.

6 of the TRMM PR products for February 1998 and February 1999, corresponding to the warm and cold phase (La Niña), respectively.

Figures 9 and 10 show the monthly mean convective, stratiform and total heating profiles derived from the SLH algorithm for six locations over the tropical oceans for February of 1998 and February of 1999, respectively. Also the CSH algorithm estimates using PR rainfall information are shown for comparison. Because the CSH algorithm estimates Q_1 due to precipitation processes, Q_1 estimated by the CSH algorithm is denoted as Q_{1p} . The SLH- and CSH-estimated mean latent heating profiles over the TOGA COARE IFA for February 1998 and February 1999 are in good agreement with each other (Fig. 9a and Fig. 10a). For February 1998, however, a secondary maximum at low-levels (~ 2 km) is found in the SLH-estimated total heating profile, while the CSH algorithm-estimated heating profiles only show one maximum heating level. This low-level maximum in the SLH-estimated total heating profile comes from the SLH-estimated convective heating profile with a low-level maximum, reflecting the abundance of shallow convection. Diagnostic budget studies over west Pacific regions (Reed and Recker, 1971; Nitta, 1972; Yanai et al., 1973; Lin and Johnson, 1996a) indicate a single heating maximum at 7–8 km altitude. The SLH-estimated mean heat-

ing profile with the low-level maximum for February 1998 does not resemble those determined from the diagnostic budget studies, while the SLH-estimated mean heating profile for February 1999 does as well as the CSH algorithm. It should be noted that diagnostic budget studies over the western Pacific do not contain periods corresponding to the warm phases of ENSO, except for two months out of the period from March to July of 1958 in Nitta (1972). Deep convection over the western Pacific is suppressed during the warm phase of ENSO (February 1998) relative to the cold phase (February 1999) due to lower sea surface temperatures. "Tradelike" regimes with abundant shallow cumulus (Johnson and Lin, 1997) are expected to be more frequent during the warm phase of ENSO (February 1998) than during the cold phase (February 1999). Thus, the difference in the SLH-estimated mean heating profile between February 1998 and February 1999 may be reasonable.

Total heating profiles over the central and eastern Pacific for February 1998 and over the south Pacific for February 1999 from the SLH algorithm also have secondary maxima at low-levels (~ 2 km), while those estimated by the CSH algorithm have a single heating maximum at 7 km altitude. Although both the SLH and CSH algorithms estimate shallow heating over the eastern Pacific for February 1999, the SLH-estimated heating peak is much sharper than the CSH-estimated one. Because it uses observed information not only on precipitation type and intensity but also on precipitation depth, the SLH algorithm estimate between shallow and deep convection are more distinct than the CSH algorithm (see S2004). Recently, Zhang et al. (2004) presented observational evidence of a shallow meridional circulation cell in the eastern tropical Pacific. The top of the shallow meridional circulation cell was found to be immediately above the atmospheric boundary layer, which may be consistent with the SLH-estimated shallow heating profile over the eastern Pacific for February 1999.

A larger difference exists between the SLH- and CSH-estimated mean heating profiles over the south Pacific for February 1998. There is a distinct double peak in the SLH-estimated heating, while the CSH-estimated heating profile shows a minimum near 4 km but not very pronounced. The SLH-estimated heating profile is very similar to the vertical distribution of heating during the undisturbed BOMEX (the Barbados Oceanographic and Meteorological Experiment) period in the trade wind belts (Nitta and Esbensen, 1974) and that during episodic trade wind regimes over the western Pacific (Johnson and Lin, 1997).

The SLH- and CSH-estimated mean latent heating profiles over the Indian Ocean for February 1998 are in good agreement with each other. On the other

hand, there are differences between the two estimates over the Indian Ocean for February 1999. The SLH-estimated mean latent heating profile has a midlevel maximum, while the CSH-estimated mean latent heating profile has a lower-level maximum. Similar differences can be found over the Atlantic Ocean for February 1998 and February 1999. These SLH-estimated heating profiles resemble the mean heating profile with a midlevel maximum that was determined from a diagnostic budget study during GATE (Thompson et al., 1979) and simulated by the GCE model (see Fig. 1b or 6b).

Generally, the SLH-estimated heating magnitudes at 7-8 km are somewhat larger than the CSH-estimated values, even if the two estimates are qualitatively in good agreement with each other. This is because the SLH-estimated heating does not include Q_R , while the CSH estimated heating does.

5. SUMMARY AND FUTURE WORK

In this study, the universality of the lookup table produced from COARE simulations used in the SLH algorithm (Shige et al., 2004) was examined for its global application to TRMM PR data. Heating profiles were reconstructed from CRM-simulated parameters (i.e. PTH, precipitation rate at the melting level, rain rate and type) with the COARE table and compared then to CRM-simulated "true" heating profiles, which were computed directly from the model thermodynamic equation. GATE, SCSMEX, and KWAJEX periods were used for the consistency check.

The consistency check indicates that the COARE table produces discrepancies between the SLH-reconstructed and GCE-simulated heating above the melting level in the convective region and at the melting level in the stratiform region. Comparisons of the COARE lookup table with those from GATE, SCSMEX, and KWAJEX simulations show that the discrepancies in the convective region are explained by differences in the vertical distribution of deeper convective heating due to the relative importance of liquid water and ice processes that varies from case to case. On the other hand, the discrepancies in the stratiform region are explained by differences in the level separating upper-level heating and lower-level cooling near the melting level.

Based on these results, algorithm improvements have been made to the SLH algorithm. In the revised procedure for convective heating retrieval, the upper-level heating amplitude due to ice processes and lower-level heating amplitude due to liquid water processes are determined separately. For stratiform regions, the heating profile is shifted up or down by matching the melting level of the COARE lookup table with the observed one. A consistency check indicates the revised SLH algorithm performs better for

each component (convective and stratiform) than the original one.

The revised SLH algorithm was applied to PR data and the results were compared to heating profiles derived diagnostically from SCSMEX sounding data (Johnson and Ciesielski, 2002). There is good agreement in the key features of the vertical profiles, particularly the level of maximum heating. The SLH-retrieved Q_{1Rp} heating magnitudes are somewhat greater than the sounding-derived magnitudes. This is caused by the fact the SLH-retrieved Q_{1Rp} does not include the Q_R implied by the sounding-derived Q_1 . Adding GCE-simulated Q_R to Q_{1Rp} provides better agreement. It was also shown that the heating estimates from PR data are subject to sampling errors due to the PR's narrow swath width (~ 215 km), leading to a discrepancy with the sounding estimates.

The revised SLH algorithm was also applied to PR data for February 1998 and February 1999, and the results were compared to heating profiles derived by the CSH algorithm (Tao et al., 1993, 2000) using PR data. Because it uses observed information not only on precipitation type and intensity but also on precipitation depth, the SLH algorithm estimates between shallow and deep convection are more distinct than the CSH algorithm (see S2004). The SLH- and CSH-estimated mean latent heating profiles over the TOGA COARE IFA for February 1998 and February 1999 are in good agreement with each other. For February 1998, however, a secondary maximum at low-levels (~ 2 km) is found in the SLH-estimated total heating profile, while the CSH algorithm-estimated heating profiles only have one maximum heating level. This low-level maximum in the SLH-estimated total heating profile comes from the SLH-estimated convective heating profile with a low-level maximum, reflecting the abundance of shallow convection. Deep convection over the western Pacific is suppressed during the warm phase of ENSO (February 1998) relative to the cold phase (February 1999) due to lower sea surface temperatures. Thus, the difference in the SLH-estimated mean heating profile between February 1998 and February 1999 may be reasonable. Total heating profiles over the central and eastern Pacific for February 1998 and over the south Pacific for February 1999 from the SLH algorithm also have secondary maxima at low-levels (~ 2 km), while those estimated by the CSH algorithm have a single heating maximum at 7 km altitude. Although both the SLH and CSH algorithms estimate shallow heating over the eastern Pacific for February 1999, the SLH-estimated heating peak is much sharper than the CSH-estimated one. The tops of shallow meridional circulation cells were found to be immediately above the atmospheric boundary in the eastern tropical Pa-

cific (Zhang et al., 2004), which may be consistent with the SLH-estimated shallow heating profiles over the eastern Pacific for February 1999. The SLH- and CSH-estimated mean latent heating profiles over the Indian Ocean for February 1998 are in good agreement with each other. On the other hand, there are differences between the two estimates over the Indian Ocean for February 1999. The SLH-estimated mean latent heating profile has a midlevel maximum, while the CSH-estimated mean latent heating profile has a lower-level maximum. Similar differences can be found over the Atlantic Ocean for February 1998 and February 1999. These SLH-estimated heating profiles resemble the mean heating profile with a midlevel maximum that was determined from a diagnostic budget study during GATE (Thompson et al., 1979) and simulated by the GCE model.

Only precipitation over oceans was considered in the current investigation. Significant differences in precipitation features between ocean and land have been shown by TRMM observations (e.g., Nesbitt et al. 2000, Petersen and Rutledge 2001, Takayabu 2002). Thus, this study will be extended to simulations of other field experiments [e.g. GAME-T (Global Energy and Water Cycle Experiment Asian Monsoon Experiment – Tropics)] in order to produce lookup tables for precipitation over land.

Acknowledgement This study is supported by the JAXA/EORC Tropical Measuring Mission (TRMM) project. The first author are grateful to Mr. Ken'ichi Ito and Mr. Masahiko Numata of RESTEC for helpful computing assistance and to Mr. Hiroshi Sasaki of Osaka Prefecture University for preparing TRMM data. Yukari N. Takayabu would like to express her hearty gratitude to late Prof. Tsuyoshi Nitta for motivating her to develop the latent heating algorithm utilizing TRMM PR data. W.-K. Tao and C.-L. Shie are mainly supported by the NASA headquarters Atmospheric Dynamics and Thermodynamics Program and the NASA TRMM. They thank Dr. R. Kakar at NASA headquarters for his support. The Grid Analysis and Display System (GrADS) package was utilized for the figures.

REFERENCES

- Awaka, J., T. Iguchi, and K. Okamoto: 1998, Early results on rain type classification by the Tropical Rainfall Measuring Mission (TRMM) precipitation radar. *Proc. 8th URSI Commission F Open Symp.*, URSI, Aveiro, Portugal, 143–146.
- Houze, R. A., Jr.: 1982, Cloud clusters and large-scale vertical motions in the tropics. *J. Meteor. Soc. Japan*, **60**, 396–410.
- 1989, Observed structure of mesoscale convec-

- tive systems and implications for large-scale heating. *Quart. J. Roy. Meteor. Soc.*, **115**, 425–461.
- Iguchi, T., T. Kozu, R. Meneghini, J. Awaka, and K. Okamoto: 2000, Rain-profiling algorithm for the TRMM precipitation radar. *J. Appl. Meteor.*, **39**, 2038–2052.
- Johnson, R. H. and P. E. Ciesielski: 2002, Characteristics of the 1998 summer monsoon onset over the northern South China Sea. *J. Meteor. Soc. Japan*, **80**, 561–578.
- Johnson, R. H. and D. C. Kriete: 1982, Thermodynamic and circulation characteristics of winter monsoon tropical mesoscale convection. *Mon. Wea. Rev.*, **110**, 1898–1911.
- Johnson, R. H. and X. Lin: 1997, Episodic trade wind regimes over the western Pacific warm pool. *J. Atmos. Sci.*, **54**, 2020–2034.
- Johnson, R. H. and G. S. Young: 1983, Heat and moisture budgets of tropical mesoscale anvil clouds. *J. Atmos. Sci.*, **40**, 2138–2146.
- Kozu, T., T. Kawanishi, H. Kuroiwa, M. Kojima, K. Oikawa, H. Kumagai, K. Okamoto, M. Okumura, H. Nakatsuka, and K. Nishikawa: 2001, Development of precipitation radar onboard the Tropical Rainfall Measuring Mission (TRMM) satellite. *IEEE Trans. Geosci. Remote Sens.*, **39**, 102–116.
- Lin, X. and R. H. Johnson: 1996a, Heating, moistening and rainfall over the western Pacific warm pool during TOGA COARE. *J. Atmos. Sci.*, **53**, 3367–3383.
- 1996b, Kinematic and thermodynamic characteristics of the flow over the western Pacific warm pool during TOGA COARE. *J. Atmos. Sci.*, **53**, 695–715.
- Mapes, B. E., P. E. Ciesielski, and R. H. Johnson: 2003, Sampling errors in rawinsonde-array budgets. *J. Atmos. Sci.*, **60**, 2697–2714.
- Nesbitt, S. W., E. J. Zipser, and D. J. Cecil: 2000, A census of precipitation features in the tropics using TRMM: Radar, ice scattering, and lightning observations. *J. Climate*, **13**, 4087–4106.
- Nitta, T.: 1972, Energy budget of wave disturbances over the Marshall Island during the years of 1956 and 1958. *J. Meteor. Soc. Japan*, **50**, 71–84.
- Nitta, T. and S. Esbensen: 1974, Heat and moisture budget analyses using BOMEX data. *Mon. Wea. Rev.*, **102**, 17–28.
- Okamoto, K.: 2003, A short history of the TRMM precipitation radar. *Cloud Systems, Hurricanes and The Tropical Rainfall Measurement Mission (TRMM): A Tribute to Dr. Joanne Simpson*, Amer. Meteor. Soc., number 51 in Meteor. Monogr, 187–195.
- Olson, W. S., C. D. Kummerow, Y. Hong, and W.-K. Tao: 1999, Atmospheric latent heating distributions in the tropics derived from satellite passive microwave radiometer measurements. *J. Appl. Meteor.*, **38**, 633–664.
- Petersen, W. A. and S. A. Rutledge: 2001, Regional variability in tropical convection: Observations from TRMM. *J. Climate*, **14**, 3566–3586.
- Reed, R. J. and E. E. Recker: 1971, Structure and properties of synoptic-scale wave disturbances in the equatorial western Pacific. *J. Atmos. Sci.*, **28**, 1117–1133.
- Shige, S., Y. N. Takayabu, W.-K. Tao, and D. E. Johnson: 2004, Spectral retrieval of latent heating profiles from TRMM PR data. Part I: Development of a model-based algorithm. *J. Appl. Meteor.*, **43**, 1095–1113.
- Takayabu, Y. N.: 2002, Spectral representation of rain features and diurnal variations observed with TRMM PR over the equatorial area. *Geophys. Res. Lett.*, **29**, doi:10.1029/2001GL014113.
- Tao, W.-K., D. Johnson, C.-L. Shie, and J. Simpson.: 2004, The atmospheric energy budget and large-scale precipitation efficiency of convective systems during TOGA COARE, GATE, SCSMEX, and ARM: Cloud-resolving model simulations. *J. Atmos. Sci.*, **61**, 2405–2423.
- Tao, W.-K., S. Lang, W. Olson, R. Meneghini, S. Yang, J. Simpson, C. Kummerow, E. Smith, and J. Halverson: 2001, Retrieved vertical profiles of latent heat release using TRMM rainfall products for February 1998. *J. Appl. Meteor.*, **40**, 957–982.
- Tao, W.-K., S. Lang, J. Simpson, and R. Adler: 1993, Retrieval algorithms for estimating the vertical profiles of latent heat release: Their applications for TRMM. *J. Meteor. Soc. Japan*, **71**, 685–700.
- Tao, W.-K., S. Lang, J. Simpson, W. Olson, D. Johnson, B. Ferrier, C. Kummerow, and R. Adler: 2000, Vertical profiles of latent heat release and their retrieval for TOGA COARE convective systems using a cloud resolving model, SSM/I, and ship-borne radar data. *J. Meteor. Soc. Japan*, **78**, 333–355.
- Tao, W.-K., C.-L. Shie, J. Simpson, S. Braun, R. H. Johnson, and P. E. Ciesielski: 2003, Convective systems over the South China Sea: Cloud-

- resolving model simulations. *J. Atmos. Sci.*, **60**, 2929–2956.
- Tao, W.-K. and J. Simpson: 1993, Goddard cumulus ensemble model. Part I: Model description. *Terr. Atmos. Oceanic Sci.*, **4**, 35–72.
- Thompson, R. M. J., S. W. Payne, E. E. Recker, and R. J. Reed: 1979, Structure and properties of synoptic-scale wave disturbances in the intertropical convergence zone of the eastern Atlantic. *J. Atmos. Sci.*, **36**, 53–72.
- Yanai, M., S. Esbensen, and J.-H. Chu: 1973, Determination of bulk properties of tropical cloud clusters from large-scale heat and moisture budgets. *J. Atmos. Sci.*, **30**, 611–627.
- Yanai, M. and R. H. Johnson: 1993, Impacts of cumulus convection on thermodynamic fields. *The Representation of Cumulus Convection in Numerical Models*, Amer. Meteor. Soc., number 46 in Meteor. Monogr., 39–62.
- Yang, S. and E. A. Smith: 1999a, Four-dimensional structure of monthly latent heating derived from SSM/I satellite measurements. *J. Climate*, **4**, 1016–1037.
- 1999b, Moisture budget analysis of TOGA COARE area using SSM/I-retrieved latent heating and large scale Q_2 estimates. *J. Atmos. Oceanic Technol.*, **16**, 633–655.
- Zhang, C., M. McGauley, and N. A. Bond: 2004, Shallow meridional circulation in the tropical eastern pacific. *J. Climate*, **17**, 133–139.